Title

Impact of the Cotton–Mouton effect on Faraday polarimetry measurements using circular polarization

Journal

Plasma Physics and Controlled Fusion, 60(8)

Author

Chen, Jie

Publication Date

2018-06-11

Peer reviewed

Impact of Cotton-Mouton Effect on Faraday Polarimetry Measurements using Circular Polarization

J. Chen, W. X. Ding and D. L. Brower

Department of Physics & Astronomy, UCLA

E-mail: chenjie@ucla.edu

May 2018

Abstract. Comprehensive understanding of the impact of Cotton-Mouton Effect on Faraday polarimetry measurements using counter-rotating circular polarization probe beams has been developed. By using Jones theory, analytic study shows the Cotton-Mouton Effect cancels to first order with coupling into the Faraday measurement only at higher orders. Jones-based numerical study shows the coupling effect strongly depends on the Cotton-Mouton Effect, Faraday Effect and wavelength chosen for the measurement. For realistic DIII-D plasma conditions and far-infrared wavelength, numerical calculation suggests the measurement is dominated by Faraday Effect while coupling effect leads to small but finite correction. By statistical comparison between experimental measurement and Jones-based numerical calculation under various plasma parameters, the impact of Cotton-Mouton Effect has been verified. Proper treatment of the coupling effect is essential in data analysis under certain conditions for polarimetric measurement using circular polarization in present devices and beyond.

1. Introduction

In tokamak research, polarimetry is a critical diagnostic which has been widely utilized in present devices and will be implemented for International-Thermonuclear-Experimental-Reactor (ITER)[1, 2]. This diagnostic passes an electro-magnetic probe beam through the plasma and measures the change of polarization of the beam, which relates to the magnetic field and electron density along the beam path. From polarimetry measurements information on the plasma density and magnetic field can be extracted, providing critical constraints for magnetic equilibrium reconstruction, input for direct feedback control, as well as important plasma parameters required for plasma physics understanding.

One of the most important issues in the application of polarimetry is to correctly interpret how the measurement is affected by coupling of various magnetic field components. There are two well-known magnetic field-induced birefringent effects in

magnetized plasmas which can change the probe beam polarization: Faraday Rotation Effect (FRE) φ_{FR} corresponding to the magnetic field parallel to the probe beam direction, and Cotton-Mouton Effect (CME) φ_{CM} corresponding to the magnetic field perpendicular to the probe beam direction:

$$\begin{aligned} \varphi_{FR} &= 2.63 \times 10^{-13} \lambda^2 \int n_e B_{\parallel} dl \\ \varphi_{CM} &= 2.46 \times 10^{-11} \lambda^3 \int n_e B_{\perp}^2 dl \end{aligned} \tag{1}$$

where λ is the probe beam wavelength in meters, n_e is the plasma density in m^{-3}, $B_{\parallel}$ and $B_{\perp}$ are the parallel and perpendicular components of magnetic field in Tesla and dl is the path length in the plasma in meters. Because of the intrinsic magnetic shear in tokamak plasma, these two effects are typically coupled, leading to potentially complicated changes in both polarization rotation and elliptization.

In general, the coupling of FRE and CME can be treated by solving the evolution of polarization using Stokes or Jones theory[3, 4]. The impact of the coupling effect is associated with the specific technical measurement approach chosen[5]. As a result, research on the coupling effect is method-dependent. For polarimetry using single probe beam with Linear-Polarization (LP), which has been commonly utilized since the early stage of tokamak research, the coupling effect has been systematically addressed previously in the literature [6, 7, 8, 9]. The coupling between FRE and CME has been found non-negligible for this technique on JET and analytic approximation of the measurement was derived under certain limiting conditions[6]. Numerical simulation was done and verified the impact of coupling of Faraday and Cotton-Mouton effects in the measurement[7, 8]. Based on this understanding, CME can be extracted from polarimetry using the LP technique and serve as an independent measurement of electron density when the perpendicular field is known. This is largely true for tokamak where $B_{\perp}$ is the toroidal magnetic field[9].

In contrast, study of the coupling effect has not been thoroughly investigated for polarimetry measurements utilizing the circular-polarization (CP) probe beam method. This approach launches two collinear counter-rotating circular-polarized probe beams into the plasma and measures Faraday Effect directly from the phase difference between the two beams[10, 11]. The virtue of this approach is manifold: it is insensitive to change of probe beam power, as it measures phase rather than amplitude; furthermore, its temporal resolution depends on the frequency difference of probe beams, which can be easily up to MHz range thereby allowing measurement of equilibrium dynamics and magnetic fluctuations[12, 13]. Consequently, polarimetry based on CP approach has been widely applied in recent years[14, 15, 16], and is going to be implemented on the ITER tangential interferometer-polarimeter system[17]. Experimentally, most observations using circular polarization technique found that FRE is dominant while coupling effect between FRE and CME are not discernible[14]. Consistently, theoretical studies have pointed out that the CME cancels to first order making the technique much less sensitive to the CME than the LP approach[18, 19]. Recent numerical work

showed polarimetry based on CP technique should experience coupling effect between FRE and CME, which might be too small to measure in present devices[20]. However, there is experimental observation where the coupling effect dominated the measurement even at low toroidal field and low electron density conditions[21]. The wavelength used in this experiment was much longer than others, suggesting wavelength plays a role in the coupling but the detailed mechanism is unclear. So far, a unified picture which can explain all previous studies is lacking for CP approach. Considering the wide application in existing and future devices, it is important to develop a comprehensive understanding of the coupling effect for CP approach.

Motivated by this need, in this paper the impact of CME on polarimetry when using CP approach has been systematically studied and the coupling effect and its mechanisms have been identified. Analytic approximation of the polarimetric measurement has been derived to show the origin of the coupling effect between FRE and CME. Parametric dependence of the coupling effect as well as the general features for a realistic tokamak plasma have been studied numerically. Most importantly, by utilizing the newly developed Radial-Interferometer-Polarimeter (RIP) on DIII-D[22], the coupling effect has been measured experimentally under various plasma conditions and systematically compared with analytic approximation and Jones theory. This paper is organized as follows: methods used in the study, including Jones theory and experimental tools, are introduced in section 2. Analytic, numerical and experimental study of the coupling effect are presented in section 3, 4 and 5 sequentially. Impact of this work is discussed in section 6.

2. Methods

Jones theory, which can be used to calculate the polarization evolution with inclusion of both FRE and CME, is adopted for this study. In polarimetry using CP approach, two collinear frequency-offset (1-2 MHz) probe beams with orthogonal right-hand-rotating (R-) and left-hand-rotating (L-) circular polarization are launched into the plasma. A linear polarizer placed in front of the detector is used to choose a specific polarization component of the probe beams emerging from the plasma. Typically, the component aligned to toroidal magnetic field is selected[19]. After the polarizer, a beat signal of the probe beams is detected from which the phase difference is obtained. Using Jones theory, the phase difference $\Delta\varphi$ can be written as:

$$\Delta\varphi = \varphi_R - \varphi_L = arg(J_{LP}\int J_p(l)dl\mathbf{e_R}) - arg(J_{LP}\int J_p(l)dl\mathbf{e_L}) \tag{2}$$

Here arg is the argument of complex number, $\mathbf{e_R}$ and $\mathbf{e_L}$ are the vectors of electric field for R and L beams, J_{LP} is the Jones matrix of linear polarizer and J_p is the Jones matrix of magnetized plasma. In Cartesian coordinates, for probe beams propagating

in z direction, the Jones matrix for a cold magnetized plasma is[4]:

$$\begin{aligned} J_p^{11} &= cos(\varphi/2) + i\frac{1-T^2}{1+T^2}sin(\varphi/2)cos(2\beta) \\ J_p^{12} &= \frac{2T^2}{1+T^2}sin(\varphi/2)sin(2\beta) + i\frac{1-T^2}{1+T^2}sin(\varphi/2)sin(2\beta) \\ J_p^{21} &= -conj(p_p^{12}) \\ J_p^{22} &= -conj(p_p^{11}) \end{aligned} \tag{3}$$

Here $conj$ is the conjugation of complex number, φ is the phase difference between characteristic waves, T is the polarization coefficient and β is the angle associated with two orthogonal perpendicular magnetic components:

$$\begin{aligned} \varphi &= \frac{\omega}{c}(\mu_+ - \mu_-)\Delta z \\ T &= \frac{\omega_{cn}^2 sin^2\gamma}{2(1-\omega_{pn}^2)cos\gamma} - \sqrt{1 + (\frac{\omega_{cn}^2 sin^2\gamma}{2(1-\omega_{pn}^2)cos\gamma})^2} \\ \beta &= tan^{-1}(\frac{B_x}{B_y}) \end{aligned} \tag{4}$$

while normalized plasma cyclotron frequency ω_{cn}, normalized electron plasma frequency ω_{pn}, refractive index of characteristic waves $\mu_\pm$ and angle associated with perpendicular and parallel magnetic components γ are defined as:

$$\begin{aligned} \omega_{cn} &= \frac{\omega_c}{\omega} = \frac{eB}{\omega m_e} \\ \omega_{pn} &= \frac{\omega_p}{\omega} = \frac{1}{\omega}\frac{e^2 n_e}{\varepsilon_0 m_e} \\ \mu_\pm^2 &= 1 - \frac{\omega_{pn}^2}{1 - \frac{\omega_{cn}^2 sin^2\gamma}{2(1-\omega_{pn}^2)} \pm \sqrt{\frac{\omega_{cn}^4 sin^4\gamma}{4(1-\omega_{pn}^2)^2} + \omega_{cn}^2 cos^2\gamma}} \\ \gamma &= tan^{-1}(\frac{\sqrt{B_x^2 + B_y^2}}{B_z}) \end{aligned} \tag{5}$$

Despite its complex form, Equation (2) reduces to a simple result when perpendicular magnetic field is zero:

$$\Delta\varphi(B_\perp = 0) = \varphi_R - \varphi_L = 2\varphi_{FR} \tag{6}$$

Which is the original principle of measurement proposed in[10]. In realistic applications, the magnetic field perpendicular to probe beams is usually not zero. The non-zero perpendicular magnetic field leads to the CME which can couple into the Faraday-effect measurement. The coupling effect can be defined as:

$$\begin{aligned} \delta &= \Delta\varphi - 2\varphi_{FR} \\ \delta_n &= \frac{\delta}{2\varphi_{FR}} \times 100\% \end{aligned} \tag{7}$$

Where δ is the coupling effect and δ_n is the coupling effect normalized by FRE, which describes the impact of coupling effect to the measurement. If perpendicular magnetic field, i.e. CME is absent, both δ and δ_n are zero. When perpendicular magnetic field is non-zero, accurate solution of Equation (2) can only be obtained numerically. To develop a comprehensive understanding of coupling effect, Equation (2) has been studied using two approaches. In section 3, Equation (2) is analytically solved under certain approximations to provide a physics picture of the origin of coupling effect. In section 4, Equation (2) is solved numerically without approximation to quantitatively reveal the general parametric dependence of coupling effect, as well as its features for a realistic plasma. Besides the analytic and numerical studies, the coupling effect has also been experimentally studied on the DIII-D tokamak. To obtain the coupling effect in experiment, the Radial Interferometer-Polarimeter (RIP) diagnostic is used to measure $\Delta\varphi$ at three different vertical positions[22], while poloidal magnetic field and electron density profiles from equilibrium reconstruction[23], constrained by Er-corrected Motion-Stark-Effect (MSE) measurement[24] as well as Thomson scattering measurement[25], is used to calculate φ_{FR} at the corresponding beam positions of RIP. Details of the experimental study are presented in section 5.

3. Analytic study

To derive a simplified analytic form of $\Delta\varphi$ from Equation (2), an assumption of uniform plasma is used in which the electron density and magnetic field are constant in space. With this assumption, the integration of Jones matrix along the probe beams is replaced by a single Jones matrix. Without loss of generality, the y axis is selected to be the direction of polarizer in front of the mixer, which is the direction of toroidal magnetic field in tokamak plasma, as mentioned earlier. From the plasma matrix, polarizer matrix and vectors for right- and left- hand rotating circular polarization, the expressions for φ_R and φ_L are obtained as:

$$\varphi_{R,L} = arctan\left[\frac{\mp\frac{2T}{1+T^2}tan(\frac{\varphi}{2}) + \frac{1-T^2}{1+T^2}tan(\frac{\varphi}{2})cos(2\beta)}{1 \pm \frac{1-T^2}{1+T^2}tan(\frac{\varphi}{2})sin(2\beta)}\right] \tag{8}$$

Assuming $\omega_{cn}, \omega_{pn} << 1$, $\mu_+ + \mu_- \approx 2$ and $\varphi_{FR}, \varphi_{CM} << 1\,rad$, approximation of Equation (8) is obtained by expanding the *arctan* and *tan* functions accurate to the 3^{rd}-order:

$$\begin{aligned}\varphi_{(R,L)_a} = \pm\varphi_{FR} + \frac{1}{2}\varphi_{CM}cos(2\beta) - \frac{1}{2}\varphi_{CM}\varphi_{FR}sin(2\beta) \mp \frac{1}{8}\varphi_{CM}^2 sin(4\beta) \\ -\frac{1}{3}\varphi_{CM}\varphi_{FR}^2 cos(2\beta) \pm \frac{1}{12}\varphi_{FR}\varphi_{CM}^2 \mp \frac{1}{4}\varphi_{FR}\varphi_{CM}^2 cos^2(2\beta)\end{aligned} \tag{9}$$

Consequently, approximation of $\Delta\varphi$ to the 3rd order is calculated:

$$\Delta\varphi_a = 2\varphi_{FR} - [\frac{1}{4}sin(4\beta) - \frac{1}{6}\varphi_{FR} + \frac{1}{2}\varphi_{FR}cos^2(2\beta)]\varphi_{CM}^2 \tag{10}$$

In the first order of $\varphi_{(R,L)_a}$, i.e. the first two terms in Equation (9), FRE has opposite sign but CME has the same sign. As a sequence, only FRE appears in the first order of $\Delta\varphi_a$ while the CME cancels, leaving $\Delta\varphi_a = 2\varphi_{FR}$ in the first order, in agreement with previous theoretical results[18, 19]. In addition, two of the second-order terms, i.e. the 3rd and 5th terms in Equation (9) also cancel. The remainder, after the subtraction, comprise the coupling effect, via the coupling between CME to FRE and β, as shown by Equation (10). Because the coupling effect only comes from higher order terms, FRE should dominate the measurement even when CME is non-negligible, as long as the assumptions above are valid. This result explains why the CP approach is largely insensitive to the CME compared to the LP approach in experiment.

As mentioned earlier, the y axis, determined by polarizer, is aligned to the direction of toroidal magnetic field. For a tokamak plasma, the toroidal magnetic field is much larger than poloidal magnetic field, i.e. $B_y >> B_x$, so that in experiment β can be approximated as zero. With this zero-β approximation, Equation (10) can be simplified to:

$$\Delta\varphi_a(\beta \approx 0) = 2\varphi_{FR} - \frac{1}{3}\varphi_{FR}\varphi_{CM}^2 \tag{11}$$

Consequently, coupling effect δ and normalized coupling effect δ_n under zero-β assumption are:

$$\begin{aligned} \delta_a(\beta \approx 0) &= -\frac{1}{3}\varphi_{FR}\varphi_{CM}^2 \\ \delta_{n,a}(\beta \approx 0) &= -\frac{1}{6}\varphi_{CM}^2 \end{aligned} \tag{12}$$

There are three implications in Equation (12). First, the coupling effect always equals to zero when FRE is zero, no matter how large the CME is; second, when FRE is not zero, the normalized coupling effect only depends on the amount of CME; last but not least, the normalized coupling effect is always negative. Correctness of these analytic results is examined in following sections.

4. Numerical study

For quantitative understanding of the coupling effect, the phase difference $\Delta\varphi$ in Equation (2) is numerically solved using different plasma parameters as input. Coupling effect δ and normalized coupling effect δ_n are then obtained by calculating φ_{FR} from Equation (1) and using Equation (7). First, a uniform plasma is used to study the general parametric dependence of coupling effect. Then, a realistic DIII-D plasma is used to explore features of the coupling effect expected in experiment.

4.1. Parametric dependence

A uniform plasma is used in the Jones-based numerical calculation and the default plasma parameters are as follows: electron density $n_e = 3 \times 10^{19}\, m^{-3}$, magnetic field

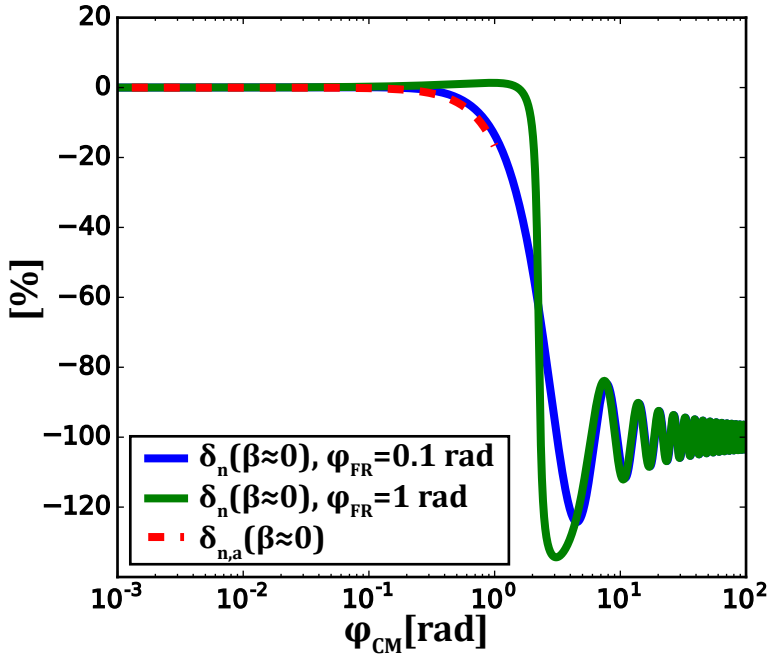

Figure 1. Under zero-β approximation: numerical solution of normalized coupling effect δ_n when $\varphi_{FR} = 0.1\,rad$ (blue line) and $\varphi_{FR} = 1\,rad$ (green line), and analytic approximation of normalized coupling effect $\delta_{n,a}$ (dash line) versus CME φ_{CM}.

$B_x = 0\,T$, $B_y = 2\,T$, $B_z = 0.1\,T$ and path length $L = 1\,m$. Note that the default setting of magnetic field corresponds to the zero-β approximation to mimic the experimental conditions. The wavelength of probe beam is chosen as $\lambda = 461\,\mu m$, as used by the RIP diagnostic on DIII-D tokamak. Probe beams propagate in z direction and polarizer is aligned to select y axis component.

The dependence of coupling effect on the CME is studied by scanning value of B_y while keeping B_z constant. The numerical solution of normalized coupling effect versus CME for cases with $\varphi_{FR} = 0.1\,rad$ and $\varphi_{FR} = 1\,rad$ is shown in Figure 1. The change of δ_n shows different stages as CME φ_{CM} increases. For both cases, when φ_{CM} is less than $0.1\,rad$, the coupling effect is negligible. As φ_{CM} increases, the normalized coupling effect become negative for both cases, indicating a negative correction to the measurement due to the coupling effect. The case of $\varphi_{FR} = 1\,rad$ has a steeper change in this process compared to case with $\varphi_{FR} = 0.1\,rad$, revealing FRE can also affect the coupling when it is large. As CME φ_{CM} exceeds $1\,rad$, the coupling fraction changes rapidly, then oscillates and saturates around -100% for both cases. δ_n at -100% corresponds to $\Delta\varphi = 0$, i.e. the polarimetric measurement completely loses the information of FRE when CME is extremely large. The negative correction of coupling effect shown by numerical calculation is in agreement with analytic zero-β approximation Equation (12). For quantitative comparison, the analytic approximation $\delta_{n,a}(\beta \approx 0)$ is calculated using Equation (12) with φ_{CM} up to $1\,rad$ and plotted in Figure 1 in dash line. Note that the analytic approximation has no FRE dependence. Good agreement is found with the numerical calculation for case with $\varphi_{FR} = 0.1\,rad$ but not for the case

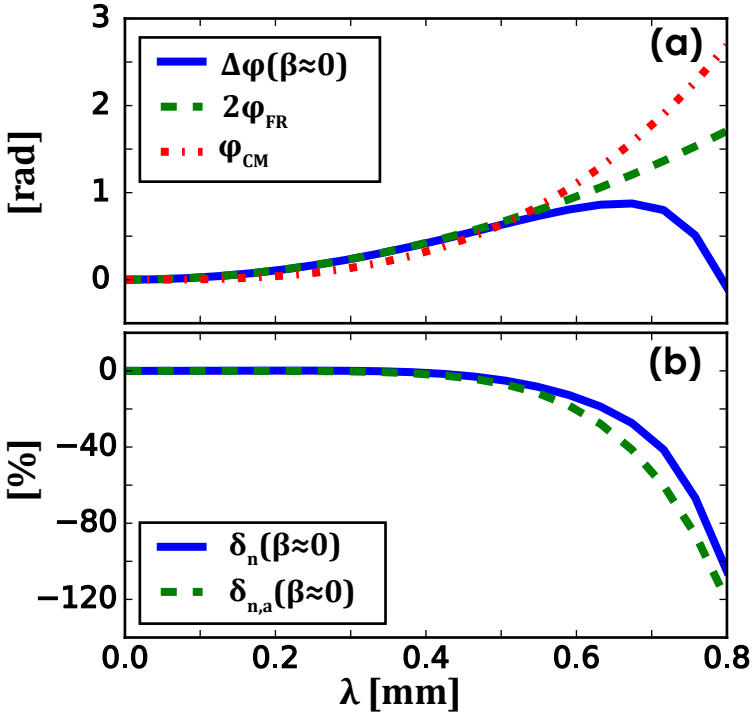

Figure 2. Under zero-β approximation: (a) Numerical solution of phase difference $\Delta\varphi$ (solid line), two times of FRE $2\varphi_{FR}$ (dash line) and CME φ_{CM} (dash-dot line) versus wavelength λ; (b) Numerical solution (solid line) and analytic approximation (dash line) of normalized coupling effect δ_n and $\delta_{n,a}$ versus wavelength λ

with $\varphi_{FR} = 1\,rad$. The discrepancy for larger φ_{FR} case is not surprising as Equation (12) is derived under the assumption that $\varphi_{FR} << 1\,rad$.

Dependence of the coupling effect on wavelength has been studied by scanning the wavelength λ while all other quantities kept constant in the numerical calculation, as shown in Figure 2. The numerical solution of phase difference $\Delta\varphi$, $2\varphi_{FR}$ and φ_{CM} versus λ is plotted in Figure 2(a). As λ increases, both φ_{FR} and φ_{CM} increase while the latter increases faster due to its stronger dependence on λ. $\Delta\varphi$ matches the trace of $2\varphi_{FR}$ when λ is less than $0.5\,mm$, and becomes smaller than $2\varphi_{FR}$ at longer wavelengths. In Figure 2(b), the numerical solution for δ_n is presented. It is less than 1% when λ is smaller than 0.3 mm, and gradually turns to -10% as λ increases to 0.6mm. When the wavelength becomes even longer, δ_n rapidly approaches -100%. The result clearly shows the coupling effect has strong dependence on wavelength and is more significant for measurements using a long wavelength source. For short wavelength, the coupling effect is negligible even when CME is large. For comparison, the analytic approximation $\delta_{n,a}(\beta \approx 0)$ is plotted in Figure 2(b), showing good consistency with the numerical calculation.

Studies described above are done under experiment-relevant zero-β approximation. For completeness, dependence of the coupling effect on β is studied by holding FRE and CME constant while changing the ratio of B_x and B_y. Practically, the scan of β is

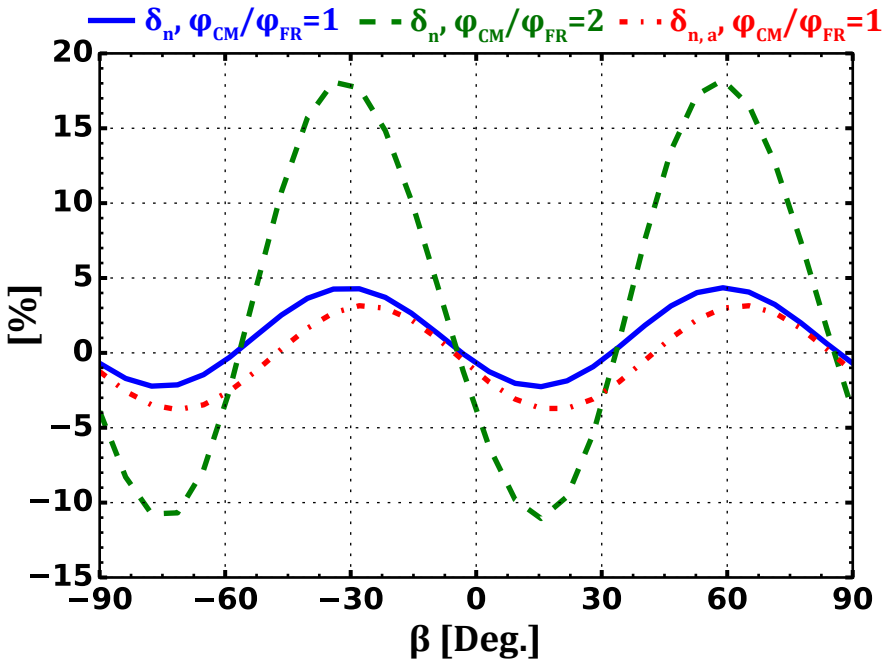

Figure 3. Numerical solution of normalized coupling effect δ_n versus β when $\varphi_{CM}/\varphi_{FR} = 1$ and $\varphi_{CM}/\varphi_{FR} = 2$. Analytic approximation of normalized coupling effect $\delta_{n,a}$ with $\varphi_{CM}/\varphi_{FR} = 1$ is shown in red dash-dot line for comparison.

equivalent to rotating the orientation of polarizer in x-y plane. In Figure 3, the numerical solution of normalized coupling effect δ_n versus β is presented for two different ratios of CME over FRE. In case with $\varphi_{CM}/\varphi_{FR} = 1$, δ_n evolves periodically from positive to negative as β changes. For certain values of β, the normalized coupling effect δ_n equals to zero. For the case $\varphi_{CM}/\varphi_{FR} = 2$, the variation of coupling fraction versus β becomes more significant and the β values corresponding to zero coupling effect are slightly changed. The periodic nature and zero-crossing point of coupling effect versus β can be understood from Equation (10): as β changes, the coupling effect will evolve with *sin* and *cos* dependences; at certain values of β, the higher order terms in Equation (10) are canceled with each other so that the total coupling effect becomes zero. Because the β values leading to cancellation depends on φ_{FR}, it is difficult to utilize this feature for minimization of the coupling effect in practice. The strong dependence of coupling effect to β reveals the importance of alignment of polarizer in the measurement. Figure 3 shows the region where β is close to zero corresponds to small δ_n in both cases,emphasizing the previously-mentioned importance of aligning polarizer to toroidal magnetic field[19]. The analytic approximation of normalized coupling effect $\delta_{n,a}$ calculated from Equation (7) and Equation (10) is plotted in Figure 3 for case $\varphi_{CM}/\varphi_{FR} = 1$, showing reasonable agreement.

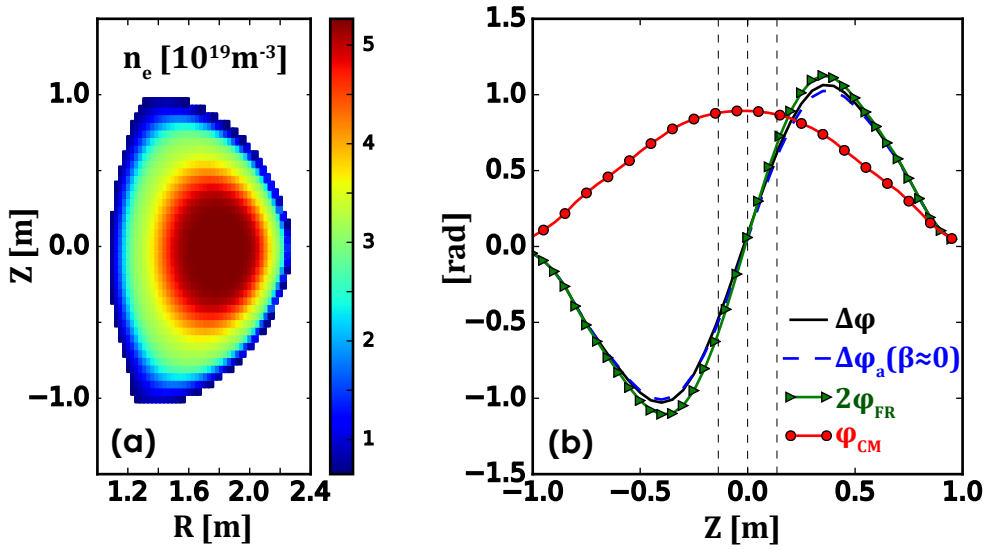

Figure 4. (a) electron density n_e profile; (b) numerical solution of phase difference $\Delta\varphi$ (solid line), analytic zero-β approximation of phase difference $\Delta\varphi_a(\beta \approx 0)$ (dash line), two times of FRE $2\varphi_{FR}$ (line with triangles) and CME φ_{CM} (line with circles) versus incident Z position of probe beams. Locations of three RIP chords are indicated by the vertical dash lines

4.2. Coupling effect in non-uniform plasma

In this part, the general features of coupling effect are explored numerically using a realistic non-uniform plasma. A typical DIII-D double-null H-mode plasma with $I_p = 1\,MA$, $B_t = 2\,T$ and $n_e = 4 \times 10^{19}\,m^{-3}$ is used. 2-D electron density profile of the plasma is shown in Figure 4(a). In the calculation, the probe beams with $461\,\mu m$ wavelength are launched horizontally from low field side and make a double pass (reflecting from a corner cube retro-reflector mounted on the inside wall), analogous to the DIII-D RIP diagnostic. The polarizer is aligned to pass the direction parallel to toroidal magnetic field. The numerical solution of phase difference $\Delta\varphi$, analytic zero-β approximation $\Delta\varphi(\beta \approx 0)$, $2\varphi_{FR}$ and φ_{CM} calculated from Equation (1) are plotted versus the launching position of probe beams in Figure 4(b).

Spatially, φ_{FR} changes sign across $Z = 0\,cm$ and peaks off-axis, because the radial magnetic field near axis is close to zero while the poloidal magnetic field changes sign across the mid-plane and is peaked at intermediate radius. φ_{CM} is peaked near axis with no sign change, due to the centrally peaked electron density and square dependence on B_T. The phase difference $\Delta\varphi$ mostly follows the trace of $2\varphi_{FR}$, even at the magnetic axis where φ_{CM} is much larger than φ_{FR}. The maximum deviation between $\Delta\varphi$ and $2\varphi_{FR}$ occurs near $Z = \pm 0.4\,m$, where both φ_{FR} and φ_{CM} are large. On the other hand, the deviation is negligible near the magnetic axis and the edge, where either or both of φ_{FR} and φ_{CM} are small. The difference between $\Delta\varphi$ and $2\varphi_{FR}$ has opposite sign when compared to $2\varphi_{FR}$, indicating a negative correction. The analytic approximation $\Delta\varphi_a(\beta \approx 0)$ shows very good agreement with numerically calculated $\Delta\varphi$, suggesting the

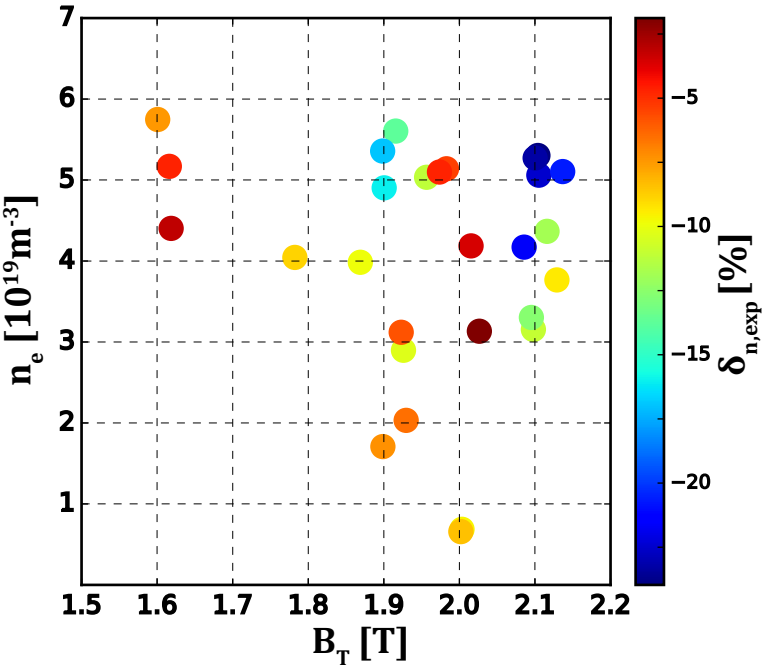

Figure 5. Experimental measurement of normalized coupling effect $\delta_{n,exp}$ (color represents the value) versus toroidal magnetic field B_T and electron density n_e

zero-β approximation is appropriate for RIP in realistic DIII-D plasmas.

5. Experimental study

Experimental measurement of the coupling effect has been accomplished in DIII-D tokamak under a broad range of plasma conditions (electron density from 0.5 to $6 \times 10^{19}\, m^{-3}$, toroidal magnetic field from 1.6 to $2.15\, T$, and plasma current from 0.8 to $1.5\, MA$ in both counter- and co-clockwise directions). As mentioned earlier, the coupling effect is experimentally determined by using RIP to provide $\Delta\varphi_{exp}$ and using EFIT to provide $\varphi_{FR,exp}$, from which $\delta_{exp} = \Delta\varphi_{exp} - 2\varphi_{FR,exp}$ and $\delta_{n,exp} = \delta_{exp}/(2\varphi_{FR,exp}) \times 100\%$ are calculated. Standard EFIT constrained by E_r-corrected MSE measurement is used, without constraint from RIP. To compare the experimental result with analytic zero-β approximation Equation (12), φ_{CM} is also calculated using EFIT. Furthermore, EFIT is also used as input of Jones-based numerical calculation to solve Equation (2) and compare with experiment measurement.

The measured normalized coupling effect $\delta_{n,exp}$ at $Z = 13.5\, cm$ under various electron densities and toroidal magnetic fields is presented in Figure 5. Despite the large range of plasma parameters, the normalized coupling effect, $\delta_{n,exp}$, is negative for all the cases under investigation, consistent with Equation (12). In general, the normalized coupling effect becomes significant as toroidal magnetic field and electron density increase, consistent with the picture that the coupling effect is from CME. When toroidal magnetic field and electron density are low, $\delta_{n,exp}$ is only about -2.5%,

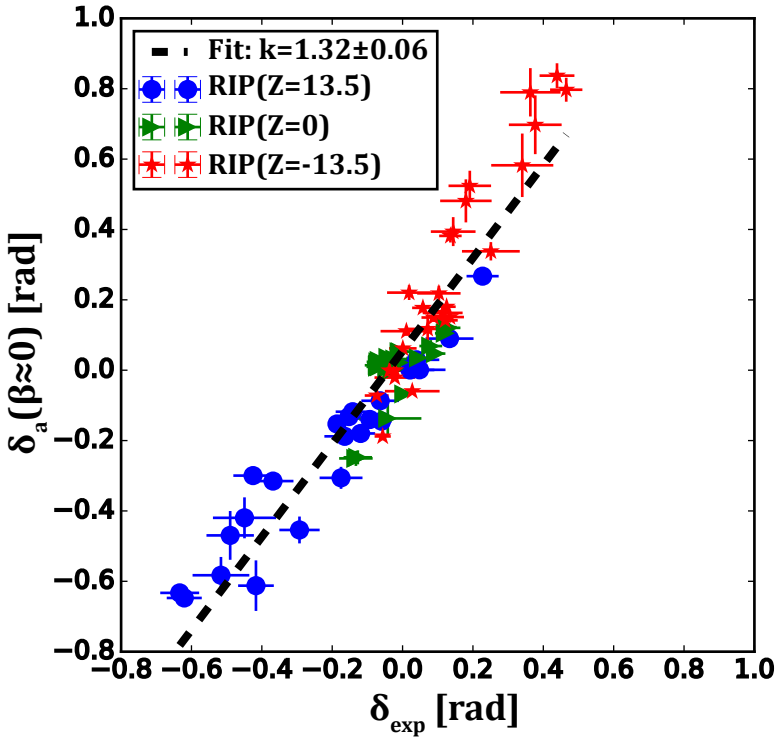

Figure 6. Experimentally measured coupling effect δ_{exp} versus analytically calculated coupling effect based on zero-β approximation $\delta_a(\beta \approx 0)$

smaller than systematic errors associated with the RIP measurement. For cases with high density and high magnetic field, $\delta_{n,exp}$ can be as large as -22.5%. Measurement at $Z = 0\,cm$ and $Z = -13.5\,cm$ shows similar features.

A direct comparison between the experimental measurement and the analytic zero-approximation of coupling effect is shown in Figure 6. The experimentally measured coupling effect δ_{exp} is plotted against the analytic approximation $\delta_a(\beta \approx 0)$ for all three horizontal positions of RIP. The experimental data uncertainty includes the Root-Mean-Square (RMS) noise and systematic errors of polarimetric measurement, while uncertainty of calculation is estimated by the uncertainty in equilibrium reconstruction and Thomson scattering measurement. Reasonable agreement is reached with a linear fit slope of 1.32 ± 0.06, suggesting the analytic approximation has 30% overestimation of the coupling effect, which is acceptable considering the assumptions involved. Direct comparison between the experimental measurement and Jones-based numerical calculation is shown in Figure 7. Despite the large range of coupling effect from -0.8 to 0.5 rad and three different horizontal positions, the measured coupling effect shows excellent linear relation to the numerical solution of coupling effect. A linear fit of the data yields a slope of 0.98 ± 0.04, which not only verifies the existence of the coupling effect, but also manifests the coupling effect is well-explained by Jones theory.

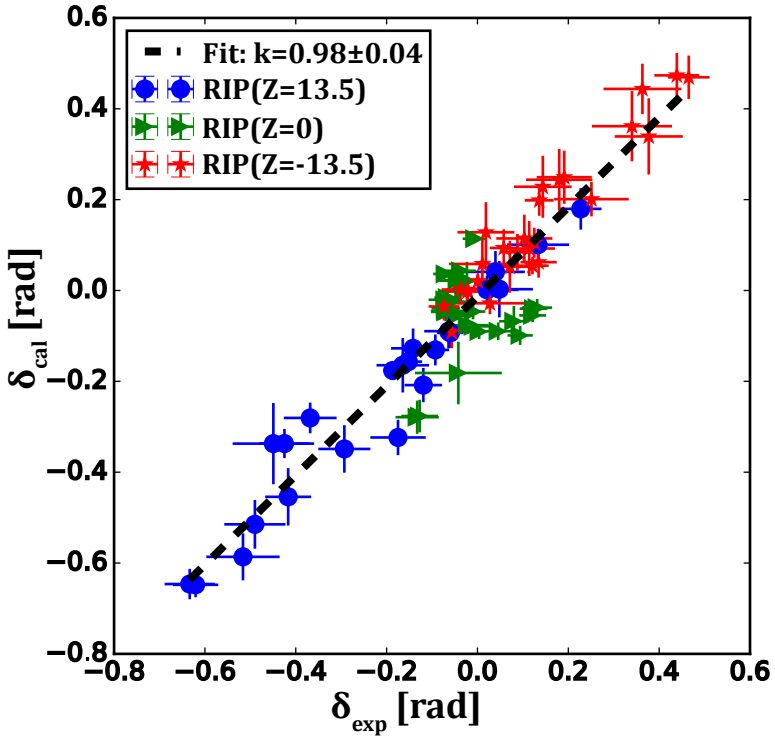

Figure 7. Experimentally measured coupling effect δ_{exp} versus numerical calculation of coupling effect δ_{cal}

6. Discussions

In previous sections, analytic, numerical and experimental study of the impact of CME on FRE measurements has been presented, providing a comprehensive understanding of the mechanism and characteristics of the coupling effect. These work help to understand previous experimental observations on several devices. Since the application of polarimetry based on CP approach, its measurement has been found mostly in agreement with expected FRE, even for the polarimeter on Alcator C-Mod where toroidal magnetic field was up to $7\,T$ and electron density greater than $1 \times 10^{20}\,m^{-3}$[14]. However, in previous DIII-D microwave polarimeter based on CP, the measurement was found heavily affected by CME[21]. From the wavelength dependence shown in Figure 2, it is clear now the difference of observation originates from different degrees of coupling. The wavelength used in C-Mod polarimeter was $118\,\mu m$, corresponding to a negligible coupling effect due to CME. On the other hand, previous DIII-D microwave polarimeter used $1000\,\mu m$ wavelength, leading to strong coupling even when electron density was low. For similar reasons, the coupling effect will be negligible for the ITER Tangential Interferometer-Polarimeter with wavelength at $10.6\,\mu m$[17]. For fixed wavelength, the coupling effect depends on level of FRE and CME, as shown by the CME dependence study. This explains the dominant FRE observed in small machines with $\varphi_{FR}, \varphi_{CM} << 1\,rad$[13, 15].

As already been shown, the impact of CME can be estimated by using the zero-β

approximation Equation (12), which provides a upper bound of the coupling effect and only requires knowledge of CME. If the coupling effect is non-negligible, such as DIII-D RIP diagnostic at moderate to high electron density and high toroidal magnetic field conditions, it should be taken into account in equilibrium reconstruction to yield a more accurate result. In addition to equilibrium measurement, polarimeter based on CP has been explored to measure magnetic fluctuation due to its fast time response[13, 22]. Quantitative analysis of the impact of coupling effect on fluctuation measurements requires detailed modelling of the magnetic fluctuation profile as well as numerical calculation using Jones theory. As a rough estimate, the fluctuation of $\Delta\varphi$ for DIII-D RIP can be obtained by linearizing Equation (11) and only keeping the first order quantities:

$$\Delta\varphi_1 = (2 - \frac{1}{3}\varphi_{CM_0}^2)\varphi_{FR_1} \tag{13}$$

Here the subscript 0 and 1 denote the equilibrium and fluctuation part of corresponding quantity. Note that for RIP, the parallel equilibrium magnetic field is small (chord at or near the magnetic axis) so that φ_{FR_0} term can be treated as a first order quantity. Equation (13) shows the polarimetric measurement is still proportional to the fluctuation of FRE even when coupling effect presents. The coupling effect only reduces the magnitude of FRE fluctuation by $\varphi_{CM_0}^2/3$, which is small unless $\varphi_{CM_0} >> 1\,rad$.

This new comprehensive understanding of the coupling effect between FRE and CME provides new insight into diagnostic development for future devices. Depending on the degree of coupling effect, there are generally two types of polarimetry based on CP approach which can have practical use in future devices. One corresponds to polarimetry with negligible coupling effect, which can be done by choosing wavelength short enough to minimize CME while keeping FRE at a proper level. As an example, for poloidal polarimeter at ITER-relevant conditions with $B_T = 5.3\,T$, $B_p = 0.5\,T$, $n_e = 1 \times 10^{20}\,m^{-3}$ and path length $L = 8\,m$(minor radius $a = 2\,m$, double-pass), choosing wavelength $\lambda = 60\,\mu m$ can lead to $\varphi_{FR} = 0.4\,rad$ while normalized coupling effect δ_n, i.e. relative error due to CME, is less than 0.1%. This coupling-free polarimetry can provide a direct measurement of FRE without requirement of additional modelling and correction. Considering the difficulty to correct the coupling effect due to the complexities such as finite temperature effect and diamagnetic effect in fusion plasma such as ITER, polarimetry measurements with negligible coupling are a strong candidate for internal magnetic field measurement. On the other hand, when accurate modelling is possible, the coupling effect could serve as a measurement and provide additional plasma information. For example, by splitting the emerging probe beams and perform the measurement with polarizers set to different orientations, FRE and CME may both be extracted by measuring coupling effect at different β.

7. Conclusions

Impact of Cotton-Mouton Effect on polarimetry using circular polarization approach has been studied systematically. An analytic approximation of the measurement accurate to 3^{rd}-order has been derived, showing the Cotton-Mouton Effect cancels to first order and couples to Faraday Effect at higher order. Numerical calculation based on Jones theory shows strong correlation of the coupling effect to the measurement wavelength, as well as magnitude of Faraday Effect and Cotton-Mouton Effect.

The coupling effect has been experimentally measured on the DIII-D tokamak, showing excellent agreement with the Jones theory. This new comprehensive description of coupling effect provides a unified understanding of previous polarimetric measurements on several devices. This work emphasizes the importance of modelling to explain measurement of present polarimeters under certain conditions as well as provides new insights into diagnostic development for future devices.

This work is supported by the U.S. DOE under Grant Nos. DE-FG03-01ER546151 and DE-FC02-04ER54698, as well as by the National Natural Science Foundation of China under Grant No. 11605067. DIII-D data shown in this paper can be obtained in digital format by following the links at https://fusion.gat.com/global/D3D_DMP.

References

[1] A. J. H. Donné, A. E. Costley, R. Barnsley, H. Bindslev, R. Boivin, G. Conway, R. Fisher, R. Giannella, H. Hartfuss, M. G. von Hellermann, E. Hodgson, L. C. Ingesson, K. Itami, D. Johnson, Y. Kawano, T. Kondoh, A. Krasilnikov, Y. Kusama, A. Litnovsky, P. Lotte, P. Nielsen, T. Nishitani, F. Orsitto, B. J. Peterson, G. Razdobarin, J. Sanchez, M. Sasao, T. Sugie, G. Vayakis, V. Voitsenya, K. Vukolov, C. Walker, K. Young, and the ITPA Topical Group on Diagnostics. Chapter 7: Diagnostics. *Nucl. Fusion*, 47(6):S337, 2007.

[2] A. J. H. Donné. Diagnostics for current density and radial electric field measurements: overview and recent trends. *Plasma Phys. Control. Fusion*, 44(12B):B137, 2002.

[3] Sergio E. Segre. A review of plasma polarimetry - theory and methods. *Plasma Phys. Control. Fusion*, 41(2):R57, 1999.

[4] H. Soltwisch. Application of Jones matrices to the analysis of far-infrared wave propagation in Tokamak plasmas. *Plasma Phys. Control. Fusion*, 35(12):1777, 1993.

[5] A. J. H. Donné. High spatial resolution interferometry and polarimetry in hot plasmas. *Review of Scientific Instruments*, 66(6):3407–3423, June 1995.

[6] K. Guenther and JET-EFDA Contributors. Approximate method to extract the pure Faraday and Cotton–Mouton effects from polarimetry measurements in a tokamak. *Plasma Phys. Control. Fusion*, 46(9):1423, 2004.

[7] F. P. Orsitto, A. Boboc, C. Mazzotta, E. Giovannozzi, L. Zabeo, and JET EFDA Contributors. Modelling of polarimetry measurements at JET. *Plasma Phys. Control. Fusion*, 50(11):115009, 2008.

[8] F. P. Orsitto, A. Boboc, P. Gaudio, M. Gelfusa, E. Giovannozzi, C. Mazzotta, A. Murari, and JET EFDA Contributors. Analysis of Faraday rotation in JET polarimetric measurements. *Plasma Phys. Control. Fusion*, 53(3):035001, 2011.

[9] A. Boboc, B. Bieg, R. Felton, S. Dalley, and Yu. Kravtsov. Invited Article: A novel calibration method for the JET real-time far infrared polarimeter and integration of polarimetry-based line-integrated density measurements for machine protection of a fusion plant. *Review of Scientific Instruments*, 86(9):091301, September 2015.

[10] G. Dodel and W. Kunz. A far-infrared 'polari-interferometer' for simultaneous electron density and magnetic field measurements in plasmas. *Infrared Physics*, 18(5-6):773–776, December 1978.

[11] D. L. Brower, W. X. Ding, S. D. Terry, J. K. Anderson, T. M. Biewer, B. E. Chapman, D. Craig, C. B. Forest, S. C. Prager, and J. S. Sarff. Laser polarimetric measurement of equilibrium and fluctuating magnetic fields in a reversed field pinch (invited). *Review of Scientific Instruments*, 74(3):1534–1540, March 2003.

[12] D. L. Brower, W. X. Ding, S. D. Terry, J. K. Anderson, T. M. Biewer, B. E. Chapman, D. Craig, C. B. Forest, S. C. Prager, and J. S. Sarff. Measurement of the Current-Density Profile and Plasma Dynamics in the Reversed-Field Pinch. *Phys. Rev. Lett.*, 88(18):185005, April 2002.

[13] W. X. Ding, D. L. Brower, S. D. Terry, D. Craig, S. C. Prager, J. S. Sarff, and J. C. Wright. Measurement of Internal Magnetic Field Fluctuations in a Reversed-Field Pinch by Faraday Rotation. *Phys. Rev. Lett.*, 90(3):035002, January 2003.

[14] W. F. Bergerson, P. Xu, J. H. Irby, D. L. Brower, W. X. Ding, and E. S. Marmar. Far-infrared polarimetry diagnostic for measurement of internal magnetic field dynamics and fluctuations in the C-MOD Tokamak (invited). *Review of Scientific Instruments*, 83(10):10E316, 2012.

[15] J. Chen, G. Zhuang, Q. Li, Y. Liu, L. Gao, Y. N. Zhou, X. Jian, C. Y. Xiong, Z. J. Wang, D. L. Brower, and W. X. Ding. High resolution polarimeter-interferometer system for fast equilibrium dynamics and MHD instability studies on Joint-TEXT tokamak (invited). *Review of Scientific Instruments*, 85(11):11D303, August 2014.

[16] H. Q. Liu, J. P. Qian, Y. X. Jie, W. X. Ding, D. L. Brower, Z. Y. Zou, W. M. Li, H. Lian, S. X. Wang, Y. Yang, L. Zeng, T. Lan, Y. Yao, L. Q. Hu, X. D. Zhang, and B. N. Wan. Initial measurements of plasma current and electron density profiles using a polarimeter/interferometer (POINT) for long pulse operation in EAST (invited). *Review of Scientific Instruments*, 87(11):11D903, November 2016.

[17] M. A. Van Zeeland, R. L. Boivin, D. L. Brower, T. N. Carlstrom, J. A. Chavez, W. X. Ding, R. Feder, D. Johnson, L. Lin, R. C. O'Neill, and C. Watts. Conceptual design of the tangentially viewing combined interferometer-polarimeter for ITER density measurements. *Review of Scientific Instruments*, 84(4):043501, April 2013.

[18] B. W. Rice. Poloidal magnetic field profile measurements on the microwave tokamak experiment using far-infrared polarimetry. 1992.

[19] J. H. Rommers and J. Howard. A new scheme for heterodyne polarimetry with high temporal resolution. *Plasma Phys. Control. Fusion*, 38(10):1805, 1996.

[20] Ryota Imazawa, Yasunori Kawano, and Kiyoshi Itami. Theoretical and numerical evaluation of polarimeter using counter-circularly-polarized-probing-laser under the coupling between Faraday

and Cotton-Mouton effect. *Review of Scientific Instruments*, 87(4):043512, April 2016.

[21] J. Zhang, W. A. Peebles, N. A. Crocker, T. A. Carter, E. J. Doyle, A. W. Hyatt, T. L. Rhodes, G. Wang, and L. Zeng. Experimental validation of Mueller-Stokes theory and investigation of the influence of the Cotton-Mouton effect on polarimetry in a magnetized fusion plasma. *Physics of Plasmas*, 20(10):102519, October 2013.

[22] J. Chen, W. X. Ding, D. L. Brower, D. Finkenthal, C. Muscatello, D. Taussig, and R. Boivin. Faraday-effect polarimeter diagnostic for internal magnetic field fluctuation measurements in DIII-D. *Review of Scientific Instruments*, 87(11):11E108, November 2016.

[23] L. L. Lao, H. E. St John, Q. Peng, J. R. Ferron, E. J. Strait, T. S. Taylor, W. H. Meyer, C. Zhang, and K. I. You. MHD Equilibrium Reconstruction in the DIII-D Tokamak. *FST*, 48(2):968–977, October 2005.

[24] T. C. Luce, C. C. Petty, W. H. Meyer, C. T. Holcomb, K. H. Burrell, and L. J. Bergsten. Method for correction of measured polarization angles from motional Stark effect spectroscopy for the effects of electric fields. *Plasma Phys. Control. Fusion*, 58(12):125010, 2016.

[25] T. N. Carlstrom, G. L. Campbell, J. C. DeBoo, R. Evanko, J. Evans, C. M. Greenfield, J. Haskovec, C. L. Hsieh, E. McKee, R. T. Snider, R. Stockdale, P. K. Trost, and M. P. Thomas. Design and operation of the multipulse Thomson scattering diagnostic on DIII-D (invited). *Review of Scientific Instruments*, 63(10):4901–4906, October 1992.